The Nature of V838 Mon and its Light Echo
ASP Conference Series, Vol. 363, 2007
R. L. M. Corradi and U. Munari eds.

HST Polarimetry of the V838 Mon Light Echo

William B. Sparks

Space Telescope Science Institute, 3700 San Martin Drive, Baltimore, MD 2128 USA

Abstract. The Advanced Camera for Surveys on-board the Hubble Space Telescope was used to obtain imaging polarimetry of the light echo of V838 Mon at four different epochs. The results from an ongoing analysis of these observations are presented and a geometric distance estimate of 5.9 kpc is derived.

1. Introduction

Distance estimation is a classical, important problem in astronomy. Traditional methods, such as the Cepheid variable period/luminosity relationship almost exclusively use flux-calibrated standard candles to derive distances. Knowing the intrinsic source brightness, its apparent brightness gives the distance. The calibration of such methods can be difficult, and prone to compounding errors as one moves to larger distances. On the other hand, if it is possible to measure the angular size of a target whose metric size is known (a "standard rod"), then a geometric distance can be inferred without many of the calibration concerns of the standard candle approach. Sparks (1994) proposed that light echo polarimetry offers just such a way to estimate geometric distances.

Following the unusual outburst of V838 Mon in 2002, and the subsequent development of its spectacular light echo, we were presented with a superb, unique opportunity both to validate this idea and to contribute significantly to an understanding of this extraordinary object by determining its distance.

Galactic light echoes are rare. The last well-studied and only other known example of similar extent to the V838 Mon light echo was that of Nova Per 1901, GK Per (Kapteyn 1901). A spectacular series of images of these echoes is presented by Ritchey (1902) showing their time evolution. There was even an attempt by Perrine (1902) to detect polarized emission from the nebulosity, however the plates, taken over several nights, are of inadequate quality to find polarized light. Following some early misunderstandings at that time, the light echo geometry was properly described by Couderc (1939).

Perhaps the most famous light echoes are the expanding "ring echoes" of SN1987A (Crotts 1988; Xu, Crotts, & Kunkel 1995). Fig. 13 of the latter reference illustrates the three dimensional geometry of these particular echoes, and shows that these rings are unlikely to be useful in determining the distance to SN1987A. They are all large, relatively bright, forward-scattered rings which define the intersection of the paraboloid surface of the echo with *sheets* of material between us and the supernova.

The peculiar supernova, SN1991T in NGC4527 in the Virgo cluster was found to host a late time optical counterpart which was shown to be a light echo.

The first clue was that its light curve ceased to decline, and next, its integrated spectrum was shown to be well-matched to the time integrated spectrum of the supernova, along with a modest "bluening" due to the increased scattering at shorter wavelengths (Schmidt et al. 1994). Sparks et al (1999) used the Faint Object Camera (FOC) on the Hubble Space Telescope (HST) to reveal extended polarized emission and derive an estimate of its distance.

For V838 Mon, distance estimates have ranged from 300 pc to 12 kpc. The nature of the outburst remains a mystery. At brightest, for plausible distance estimates, V838 Mon was likely to have been the most luminous star in the Galaxy. To constrain its nature, history and environment, knowledge of the distance is critical.

2. Light Echoes Properties and Polarization

When a nova or supernova explodes, it can be considered as an extremely intense point-source flash of light. The details of the explosion physics are not relevant – what matters is that the event is *bright* and is *localized* in time and space. The flash is radiated essentially isotropically, and expands into the surrounding interstellar medium where it will encounter dust grains and be scattered. A portion of the scattered light travels towards the Earth and arrives at time t after the initial outburst, given by the extra path length d traversed, such that $t = d/c$. At fixed time t the surface corresponding to the additional path is an ellipsoid (almost parabaloid) with one focus at the explosion and the other at the observer. If z is the line-of-sight distance then

$$z = \frac{(ct)^2 - x^2}{2ct}$$

where x is the coordinate in the plane of the sky (Couderc 1939, Chevalier 1986, Sparks 1994). Light that travels in the plane of the sky containing the outbursting star, $z = 0$, is scattered by 90° at radius $x = ct$. While the *intensity* of scattered light depends on dust density, attenuation, and phase function, the *polarization degree* should be quite simple. There is a 1:1 correspondence between angular radius and scattering angle, and polarization degree maximizes at 90° scattering, see Fig. 1.

Sparks (1997) and Sugerman (2003), summarize quantitative expressions for light echo properties. The angular diameter from which the distance is obtained is

$$\phi = 0.126\ (t\ \mathrm{yr}/D\ \mathrm{Mpc})\ \mathrm{arcsec}.$$

If the time of the event is not known, the echo may still yield the distance, since the transverse velocity of the ring of maximum polarization is c and hence the apparent expansion rate gives the distance (Sparks 1996) through

$$d\phi/dt = 1.73(6kpc/D)\ \mathrm{arcsec}/30\ \mathrm{day} = 1.6(H_0/75)/(z/0.02)\ \mathrm{mas/yr}.$$

For an instantaneous light flash, the echo surface is an ellipsoid with the flash at one focus and the observer at the other. Because of the extremes of astronomical distances, this ellipsoid is well-approximated by a paraboloid, assumed adequate for the remainder of this contribution. The primary complication in the case of

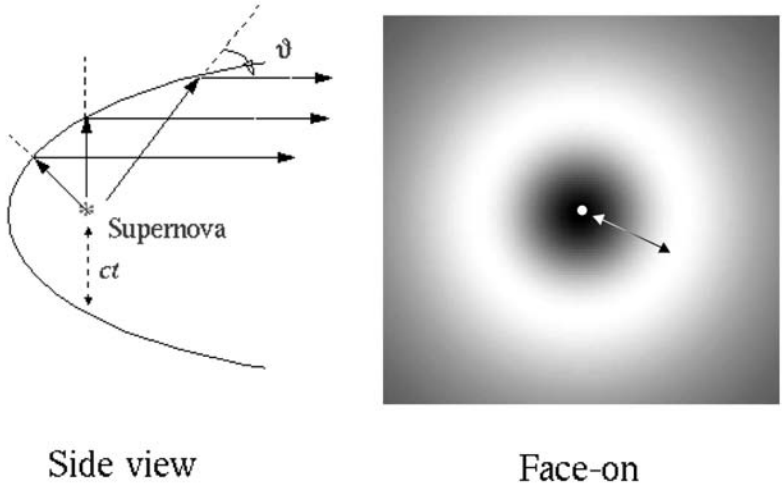


Figure 1. Schematic of the geometry of a light echo. The left hand view shows a section through the light echo from the side, while the right hand panel shows the polarization degree viewed face-on.

the V838 Mon light echo is the extended duration of the outburst relative to the timescales involved, and we use full three dimensional modelling of the echo rather than short-duration δ-function approximations with analytic expressions (Sparks 1994; Sugerman 2003).

3. Observations and Data Processing

3.1. Observations

Polarization images of the V838 Mon light echo were obtained using the Wide Field Camera (WFC) of the Advanced Camera for Surveys (ACS) on board the Hubble Space Telescope (HST) during 2002 and again in 2005. To make polarization observations, the echo was imaged with the F606W filter in beam and successively with the three visual, "POL_V", polarizers which are oriented at nominal position angles of 0, 60 and 120 degrees, though with a zeropoint offset in position angle. The polarizer filters are designed to fill the field-of-view of the High Resolution Channel (HRC), but not the WFC, and hence the polarization images are configured to almost fill one quadrant of the WFC camera. The readout image is one quadrant of the full WFC field of view. Specifically, polarization images were obtained 20th May, 2002, 2nd September 2002, 17th December 2002 and 16th December 2005. We focus primarily on the December 2002 series in this work.

3.2. Data processing procedures

The data were pre-processed through the STScI calibration pipeline in order to debias and flat-field the individual images. To simultaneously remove cosmic rays, correct for geometric distortion and register images spatially, the task "multidrizzle" was used in stand-alone mode within stsdas/pyraf. The final images were rectified onto a spatial grid with pixel size 0.05 arcsec, and the location of V838 Mon within each frame was registered for all polarizer images at each epoch. Because of optical power on the polarizers, the geometric corrections are unique for each polarizer. Small image offsets are also introduced by the polarizers but then removed in HST pointing control software.

For polarization processing, we kept the data in detector coordinates since the polarizer position angles are fixed in detector coordinates. The three Stokes parameters, I (the total intensity), Q and U (the linear polarization parts of the Stokes polarization vector) are derived using linear combinations of the three images obtained with the polarizing elements in beam (see e.g. Collett 1992 and Tinbergen 1996 for basic polarization concepts). For perfectly efficient ideal polarizers oriented at relative position angles of 60 degrees, we used the formulae and conventions for the Stokes parameters, where r is the source countrate and the subscript identifies the particular polarizer:

$$I = \frac{2}{3}(r_0 + r_{60} + r_{120})$$

$$Q = \frac{2}{3}(2r_0 - r_{60} - r_{120})$$

$$U = \frac{2}{\sqrt{3}}(r_{120} - r_{60})$$

From the Stokes parameters, we derived the polarization degree p:

$$p = \sqrt{Q^2 + U^2}/I$$

together with the polarization electric vector position angle in detector coordinates, θ_D

$$\theta_d = \frac{1}{2} atan(\frac{U}{Q}) + 51.8$$

where the 51.8 degree zeropoint is the orientation of the POL0 polarizer projected onto the WFC detector (Biretta et al. 2004; Platais & Biretta 2004).

Each of the individual polarizers in fact has a unique transmittance, and we corrected for this using the calibration measurements in Biretta et al. (2004). We further assumed the efficiency of each polarizer (their ability to block light of the orthogonal polarization state) is perfect and then used the procedures described in detail in Sparks & Axon (1999). Applied to the ACS polarizers, that process uses the formulae above for perfectly efficient polarizers, though in addition requires a noise model and estimate of the underlying background sky level which are used to return estimates of the uncertainties on polarization measurement as well as debiasing the positive definite polarization flux quantity.

To estimate the underlying sky level, we measured the mean value in a selection of regions outside the echo. For the December 2005 this was not possible

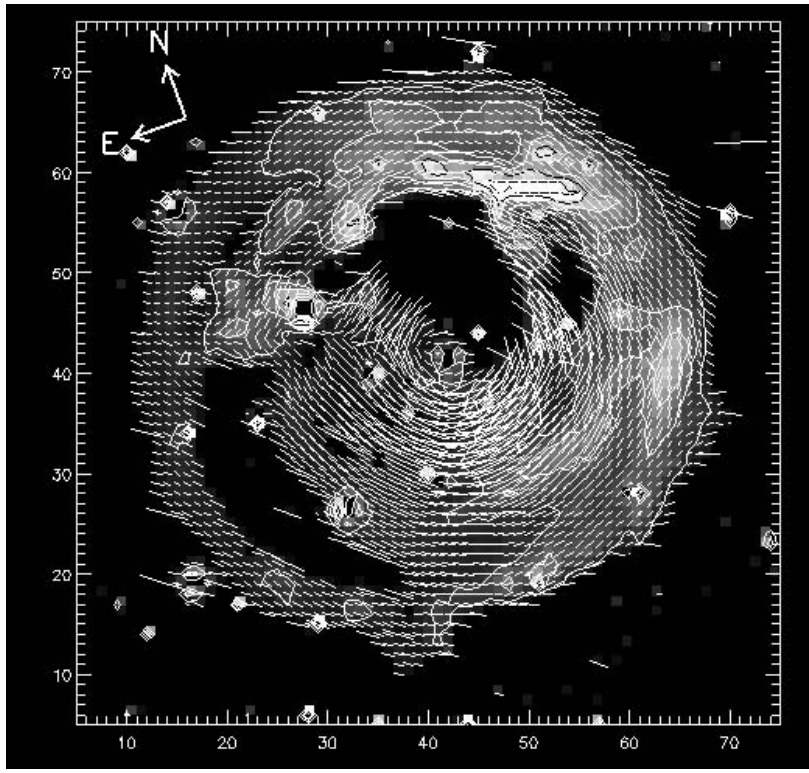


Figure 2. Image of Stokes I for V838 light echo, December 2002, with polarization degree and position angle vectors superimposed.

since the echo filled the polarizer field of view. However an unpolarized direct image was obtained using the full field of the WFC for which sky measurement was straightforward. To estimate the sky level in the polarization images, the polarized images were matched to this wider field direct image. An important step in the polarization analysis is to establish a noise model. To do this, we used the error image provided in the pipeline processing.

We checked our procedures by deriving polarization properties for calibration star observations and found polarization percentages between 5 and 7% for a star nominally polarized 6.5%. We recovered its position angle consistent to within a few degrees.

An example image with polarization vectors superimposed is shown in Fig. 2. The pattern of polarization is smooth and centrosymmetric as expected from a straightforward scattering configuration. We do not find the distortions in scattering pattern reported by Desidera et al (2004). The smooth pattern we find is reproduced from epoch to epoch, with the telescope at different orientations, which give us confidence in our processing.

For comparison to scattering models of the echo, it was necessary to clean the basic polarization images two steps further. Firstly we wished to accept only

data of good signal-to-noise level. We rejected regions of the polarization degree image having an uncertainty greater than 15% of the polarization degree; that is regions with a signal-to-noise ratio S/N less than 6.7. Also, the presence of a substantial number of stars in the field of view also influences the images of polarization degree. We eliminated regions of the data where the stellar halos exceeded 15% of the total Stokes I intensity and which hence could depress the apparent polarization degree by 15% or more.

4. Modelling the Light Echo

For a given distance to V838 Mon, the geometry is fully specified. Each point of time in the outburst light curve maps onto its own paraboloid surface, and hence down any given line of sight, we see a slightly distorted version of the light curve. The front part of the echo along a line of sight, being nearest us, corresponds to the least amount of time delay hence the end of the outburst, while the longest time delay, at the back of the line of sight, corresponds to the beginning of the outburst. The total extent of the outburst maps onto a spatial range in z down the line-of-sight, and that range changes with angular radius from the star.

We modelled this behaviour using an empirical light curve, where each time corresponds to a separate paraboloid surface. To this initial three dimensional "source function", we added a Henyey-Greenstein (1941) scattering phase function to allow for the geometric scattering angle dependence of scattering efficiency (dust is quite strongly forward-scattering), and then we further modified the three dimensional source function to determine the contribution at each point down the line-of-sight to the Stokes-Q parameter. We used a Rayleigh-type polarization function $p = p_{max}(1 - cos^2\theta)/(1 + cos^2\theta)$.

Integration of the total intensity scattered source function and the Stokes parameter source function down the line of sight gave our models for comparison to data, with free parameters which are the dust density and the maximum degree of polarization p_{max}. The models also yield an intensity weighted mean scattering angle for each radius, on the assumption of uniform density. We developed these models for a range of distances between 4 and 12 kpc for the 16th December 2002 epoch.

5. Results

Fig. 3(a) plots the empirical polarization curve derived for 16th December 2002. Overlaid on it is the model polarization for a distance of $D = 5.6$ kpc, which is the distance at which chi-squared of the model compared to the data minimizes, when the entire polarization profile is used in the fitting. The derived p_{max} in this case is 0.53, i.e. 53% peak polarization. Given a distance estimate, such as this, we then know the relationship between the angular radius from the star and the scattering angle, hence we can recast the polarization versus radius data into the form polarization versus scattering angle, which allows more direct comparison to physical models. If we do this for a distance of $D = 5.6$ kpc, we see that the peak polarization is slightly offset relative to the model, with a peak polarization at scattering angle between 90 and 100 degrees.

We therefore adopted a second approach to compare models and data, which was to only examine the region around the peak of polarization. Specifically, for a range of assumed distances, we fitted a parabola to the curve of polarization versus scattering angle for values of polarization $p > 0.3$ and looked at the mean-squared residuals from the fit. By this approach, a minimum in mean-squared residuals is obtained for a distance of $D = 5.9$ kpc, shown in Fig. 3(b).

This method is testing the symmetry of the polarization function, and an interesting quality emerges. The location of the scattering angle corresponding to the polarization peak is unconstrained, yet for the minimum mean-squared residuals, it transpires that the scattering angle of the polarization maximum is $\theta = 90.6$ deg, very close to the anticipated 90 deg scattering angle maximum for polarization. The maximum polarization of this function is 0.48, or 48% polarization.

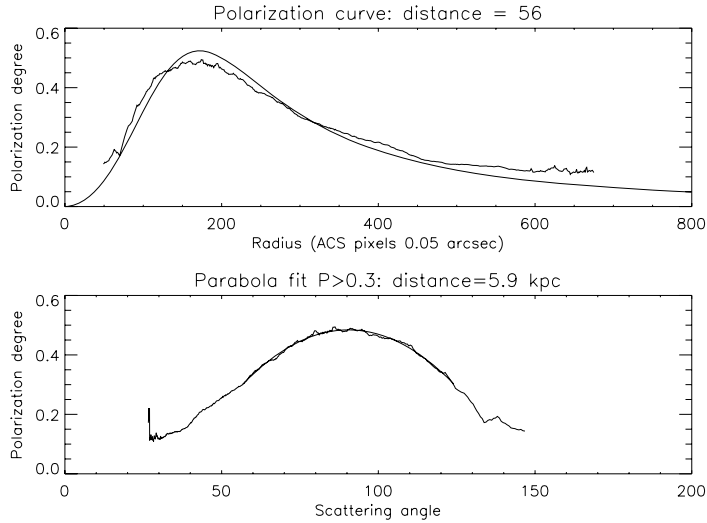


Figure 3. Above (a) shows empirical polarization versus radius for December 2002, with a best-fit model polarization curve overlaid. Below (b) the polarization is plotted against scattering angle for a best-fit distance of 5.9 kpc with parabola fitted through peak overlaid.

Finally, with our best estimate of the distance currently $D = 5.9$ kpc, we can examine how well the polarization curve does in locating the peak for the other three epochs. In the first epoch, May 2002, the ring of maximum polarization is interior to the inner edge of the gap close to V838 Mon at that time. For September 2002, it is on the edge of that gap, and consistent with its being at the appropriate angular radius (Bond et al. 2003). For December 2005, the predicted location of the ring of maximum polarization does indeed pass through a region of high polarization, though the data at that epoch are of low signal to noise. The work is ongoing and a number of instrumental effects are still under investigation, however at the time of the conference, the best distance estimate was $D = 5.9$ kpc.

6. Conclusions

We have used the concepts of Sparks (1994) to investigate the utility of imaging polarization of light echoes to derive geometric distances for the spectacular example of the V838 Mon light echo. The qualitative and quantitative behaviour of the polarization pattern is consistent with expectations, and we derive a geometrical distance to V838 Mon of D=5.9 kpc with very small random error, but a systematic error of order 5 to 10%.

The potential to use the method beyond our own galaxy is significant, to distances of order that of the Virgo cluster. All galaxies have supernovae and all galaxies have at least some interstellar material, and so with sufficient sensitivity, they should display light echoes. Only a subset of the echoes will be useful in practice, however this may be a reasonably large subset.

Acknowledgments. I acknowledge the efforts of Howard Bond, principal investigator for the data used in this work, and Misty Cracraft (STScI) who carried out much of the analysis. The work is based on observations made with the NASA/ESA *Hubble Space Telescope*, obtained at the Space Telescope Science Institute. Support for this work was also provided by NASA through grant number GO-9694 from the Space Telescope Science Institute, which is operated by AURA, Inc., under NASA contract NAS 5-26555.

References

Biretta, J., et al. 2004, ACS Instrument Science Report, ACS ISR 2004-09
Bond, H.E., Henden, A.A., Levay, Z., Panagia, N., Sparks, W.B., Starrfield, S., Wagner, R.M., Corradi, R.L.M., Munari, U. 2003, Nature, 422, 405
Chevalier, R.A. 1986, ApJ, 308, 225
Collett, E. 1992, Polarized Light: Fundamentals and Applications, Marcel Dekker: New York
Couderc, P., 1939, Ann. d'Astrophys., 2, 271
Crotts, A.P.S. 1988, ApJ, 333, L51
Desidera, S., Giro, E., Munari, U., Efimov, Y. S., Henden, A., Benetti, S., Tomov, T., Bianchini, A., Pernechele, C. 2004, A&A, 414, 591
Henyey, L.G., Greenstein, J.L. 1941 ApJ, 93, 70
Kapteyn, J.C. 1901, Astron. Nach., 157, 201
Perrine, C.D. 1902, Apj, 16, 249
Platais, V., Biretta, J. 2004, ACS-ISR 2004-10
Ritchey, G.W. 1902, ApJ, 15, 129.
Schmidt, B.P., Kirshner, R.P., Leibundgut, B., Wells, L.A., Porter, A.C., Ruiz-Lapuente, P., Challis, P. & Filippenko, A. 1994, ApJ, 434, L19
Sparks, W.B. 1994, ApJ, 433, 29
Sparks, W.B. 1996, ApJ, 470, 195
Sparks, W.B. 1997, in "The Extragalactic Distance Scale", Space Telescope Science Institute Symp. Series 10, CUP, eds. M. Livio, M. Donahue, N. Panagia, p. 281
Sparks, W.B., Macchetto, F., Panagia, N., Boffi, F.R., Branch, D., Hazen, M.L., della Valle, M. 1999, ApJ, 523, 585
Sparks, W.B., Axon, D.J. 1999, PASP, 111, 1298
Sugerman, B.E.K. 2003, AJ, 126, 1939
Tinbergen, J. Astronomical Polarimetry, CUP 1996
Xu, J., Crotts, A.P.S. & Kunkel, W.E. 1995, ApJ, 451, 806